

## **All-inorganic 0D/3D Cs<sub>4</sub>Pb(IBr)<sub>6</sub>/CsPbI<sub>3-x</sub>Br<sub>x</sub> Mixed-dimensional Perovskite Solar Cells with Enhanced Efficiency and Stability**

Zhenzhen Li,<sup>a</sup> Xiaolong Liu,<sup>a\*</sup> Jia Xu,<sup>a</sup> Shujie Yang,<sup>a</sup> Hang Zhao,<sup>a</sup> Hui Huang,<sup>b</sup>  
Shengzhong (Frank) Liu,<sup>c\*</sup> Jianxi Yao<sup>a\*</sup>

<sup>a</sup>State Key Laboratory of Alternate Electrical Power System with Renewable Energy  
Sources, Beijing Key Laboratory of Energy Safety and Clean Utilization, North China  
Electric Power University, Beijing 102206, P. R. China

<sup>b</sup>Singapore Institute of Manufacturing Technology, 2 Fusionopolis Way, 138634,  
Singapore

<sup>c</sup>Key Laboratory of Applied Surface and Colloid Chemistry, Ministry of Education,  
Shaanxi Key Laboratory for Advanced Energy Devices, Shaanxi Engineering Lab for  
Advanced Energy Technology, School of Materials Science & Engineering, Shaanxi  
Normal University, Xi'an 710119, P. R. China

### **Corresponding Author**

\* E-mail: [jianxiyao@ncepu.edu.cn](mailto:jianxiyao@ncepu.edu.cn)

\* E-mail: [liusz@snnu.edu.cn](mailto:liusz@snnu.edu.cn)

\* E-mail: [xl.liu@ncepu.edu.cn](mailto:xl.liu@ncepu.edu.cn)

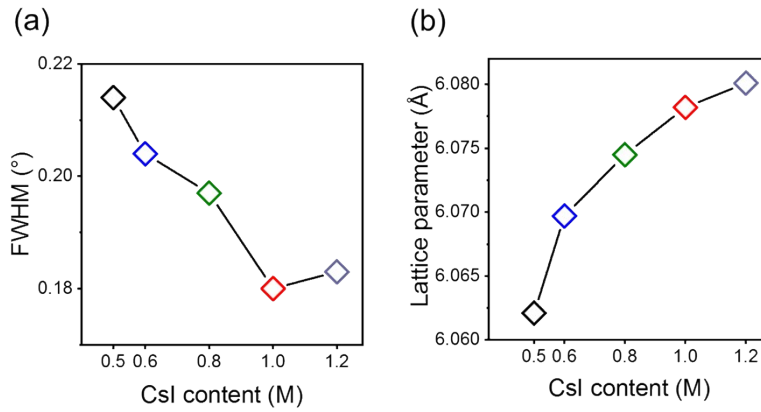


**Figure S1** (a) FWHM values of (200) peaks in XRD patterns with various CsI content  $y$  in precursors; (b) Lattice parameters of  $\text{CsPbI}_{3-x}\text{Br}_x$  in the  $y$ -CsI films.

**Table S1** Lattice parameter of  $\text{CsPbI}_{3-x}\text{Br}_x$  and  $\text{Cs}_4\text{Pb}(\text{IBr})_6$  in the  $y$ -CsI films.

Samples	$\text{CsPbI}_{3-x}\text{Br}_x$	$\text{Cs}_4\text{Pb}(\text{IBr})_6$
	(Å)	(Å)
0.5-CsI	$a = b = c = 6.0693$	--
0.6-CsI	$a = b = c = 6.0710$	--
0.8-CsI	$a = b = c = 6.0745$	$a = b = 14.3162, c = 17.9782$
1.0-CsI	$a = b = c = 6.0782$	$a = b = 14.3353, c = 18.0139$
1.2-CsI	$a = b = c = 6.0801$	$a = b = 14.3629, c = 18.0615$

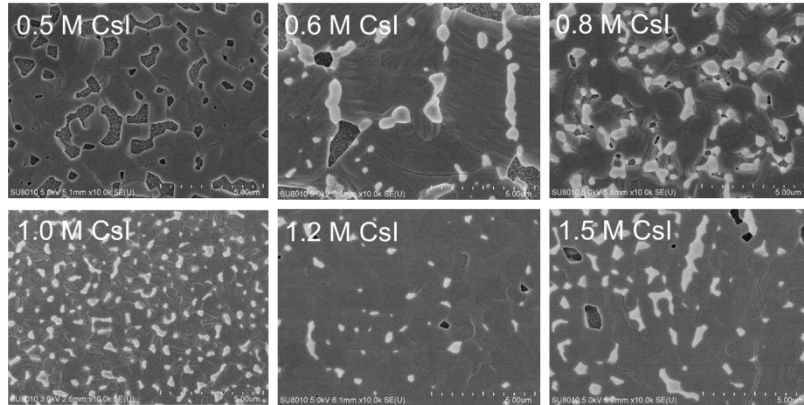


**Figure S2** SEM images of the  $\gamma$ -CsI films.

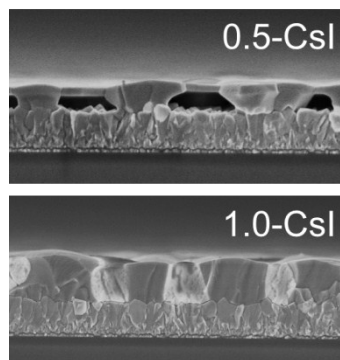


**Figure S3** SEM cross-sectional images of the 0.5-CsI and 1.0-CsI films on FTO glass substrates.

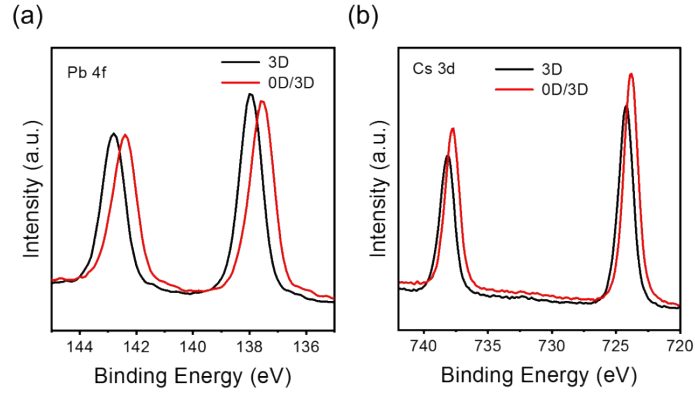


**Figure S4** XPS spectra of (a) Pb 4f and (b) Cs 3d peaks of the 0.5-CsI and 1.0-CsI films.

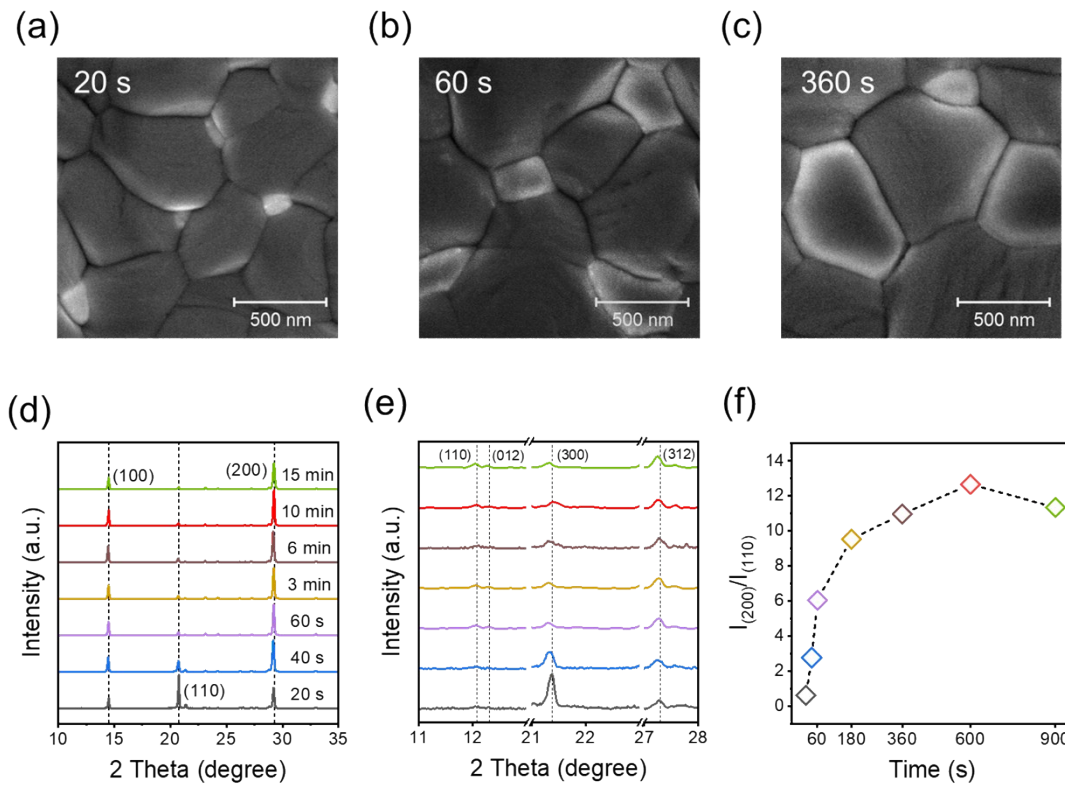


**Figure S5** SEM images of the 1.0-CsI films annealed for (a) 20 s, (b) 60 and (c) 360 s; (d) XRD patterns of the 1.0-CsI film annealed for 20 s to 15 mins; (e) Zoom-in XRD patterns of the Figure S5d; (f) The intensity ratio of  $I_{(200)}/I_{(110)}$  for the  $\gamma$ -CsI films.

**Figure S6** illustrates XRD patterns of “ $y$ -CsBr” films. Concentrations of CsI and  $\text{PbI}_2$  in precursor solutions were both fixed at 1.0 M, while concentration of CsBr varied from 0.1 to 0.7 M. When  $y$  was increased to 0.1,  $\delta$ - $\text{CsPbI}_{3-x}\text{Br}_x$  was formed, which is due to insufficient Br content to stabilize cubic  $\text{CsPbI}_{3-x}\text{Br}_x$  phase. As CsBr concentration increased to 0.3 M, characteristic peaks of the 0D  $\text{Cs}_4\text{Pb}(\text{IBr})_6$  began to appear. With increasing CsBr concentration from 0.3 to 0.7 M, a similar phenomenon was observed as in experiments with varying CsI contents, and the crystallinity of the dominant  $\alpha$ - $\text{CsPbI}_{3-x}\text{Br}_x$  was improved. Obviously enhanced (100) and (200) peaks of the  $\alpha$ - $\text{CsPbI}_{3-x}\text{Br}_x$  were observed, which suggests that relative excess  $\text{Cs}^+$  content at such elevated temperature promote formation of the 0D  $\text{Cs}_4\text{Pb}(\text{IBr})_6$  and further improve crystallization quality of the 3D  $\text{CsPbI}_{3-x}\text{Br}_x$ .

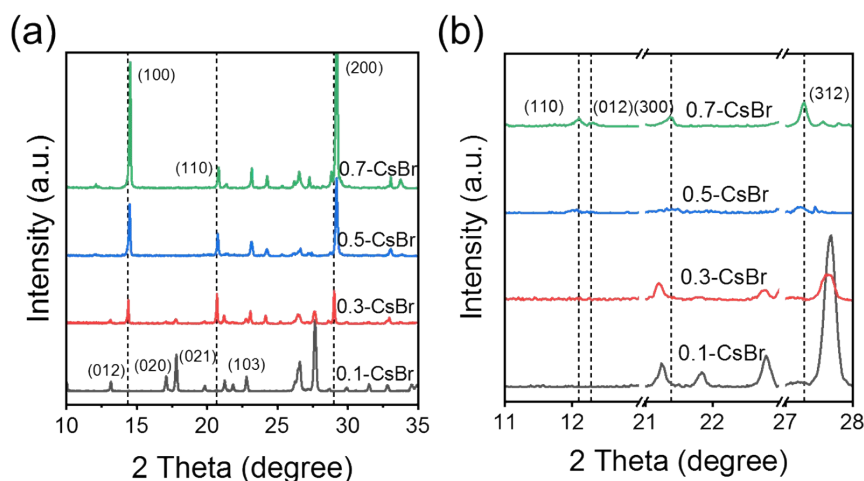


**Figure S6** (a) XRD and (b) Zoom-in XRD patterns of the 0.1-CsBr, 0.3-CsBr, 0.5-CsBr and 0.7-CsBr films.

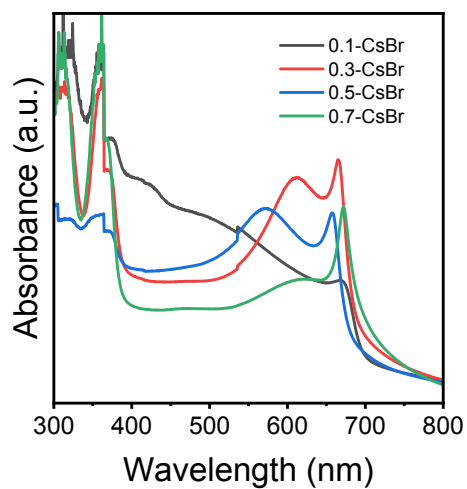


**Figure S7** UV-Vis spectra of the  $\gamma$ -CsBr films.

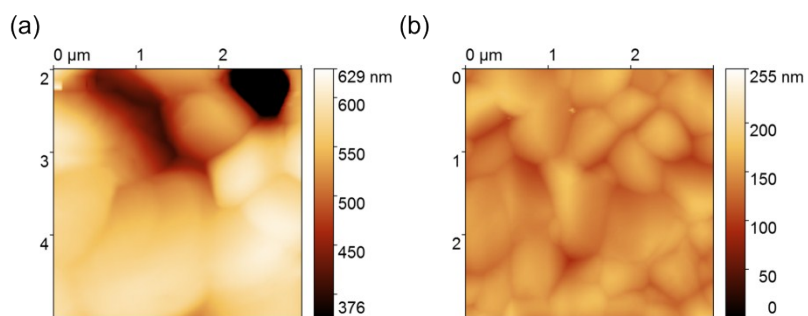


**Figure S8** KPFM topographical images of (a) 3D and (b) 0D/3D  $\gamma$ -CsI films.

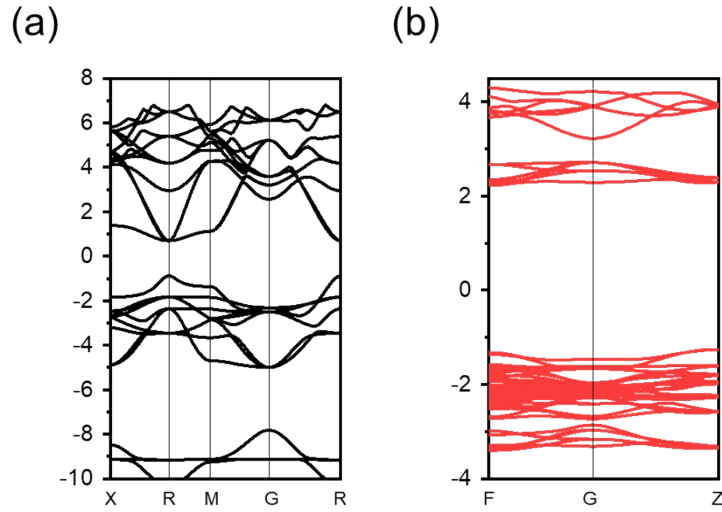


**Figure S9** Conduction band minimum (CBM) and valence band maximum (VBM) for **(a)**  $\text{CsPbI}_{3-x}\text{Br}_x$  and **(b)**  $\text{Cs}_4\text{Pb}(\text{IBr})_6$  obtained by DFT calculations.

**Table S2** Bi-exponential fitted parameters for TRPL of the  $y$ -CsI films.

	$\tau_1$ (ns)	$\tau_2$ (ns)	$\tau_{\text{avg}}$ (ns)	A1 (%)	A2 (%)
0.5-CsI	2.588	6.222	4.291	53.129	46.871
0.6-CsI	1.663	5.786	4.785	24.282	75.718
0.8-CsI	1.501	7.970	6.990	12.821	87.179
1.0-CsI	0.578	8.963	8.696	3.185	96.815
1.2-CsI	0	8.422	8.422	0	100

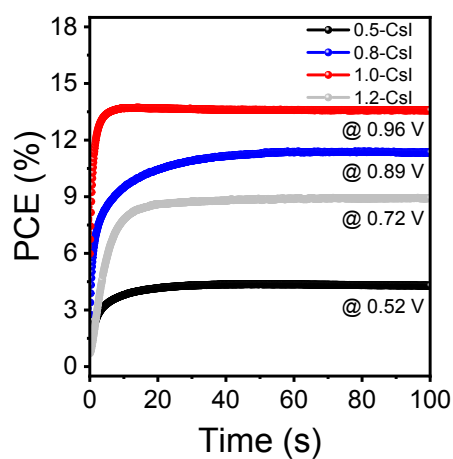


**Figure S10** Stabilized power output of corresponding PSCs based on the  $\gamma$ -CsI films.

**Table S3** Comparison of performance parameters for PSCs based on the  $\gamma$ -CsI films.

	$J_{sc}$	$V_{oc}$	$FF$	PCE	$J_{sc}$	$V_{oc}$	$FF$	PCE
	( $mA\ cm^{-2}$ )	(V)	(%)	(%)	( $mA\ cm^{-2}$ )	(V)	(%)	(%)
	Forward				Reverse			
0.5-CsI	10.52	0.62	32.61	2.13	10.57	0.72	60.96	4.64
0.8-CsI	14.43	0.91	72.44	9.53	15.50	1.05	76.94	12.57
1.0-CsI	15.05	1.07	76.01	12.32	16.56	1.11	80.32	14.77
1.2-CsI	14.20	0.85	71.94	8.68	14.33	0.89	71.55	9.17



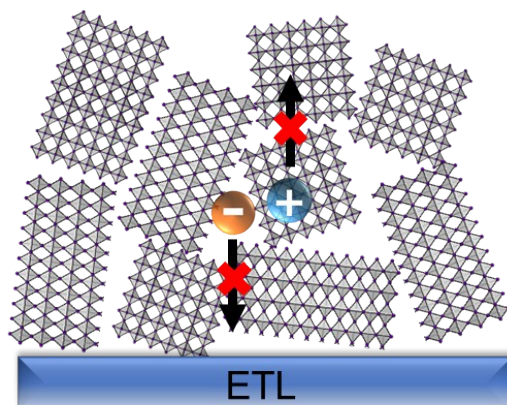


**Figure S11** Illustration of carrier transport in PSCs based on the 3D 0.5-CsI film with random crystal orientation.

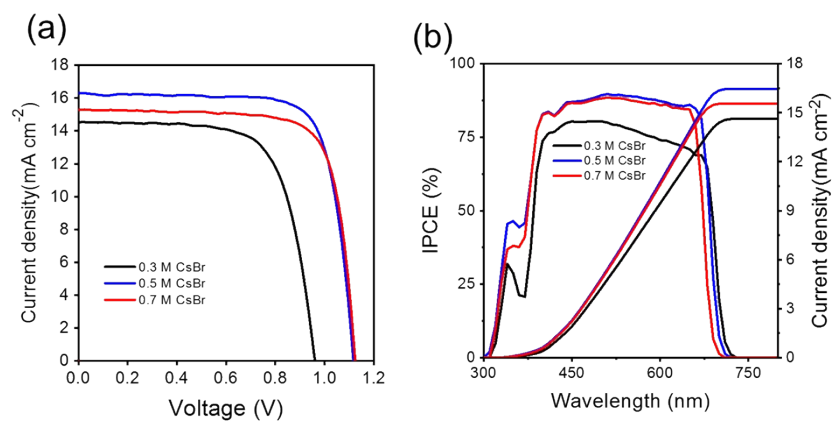


**Figure S12 (a)** *J-V* curves, **(b)** IPCE spectra of corresponding solar cells based on *y*-CsBr films.

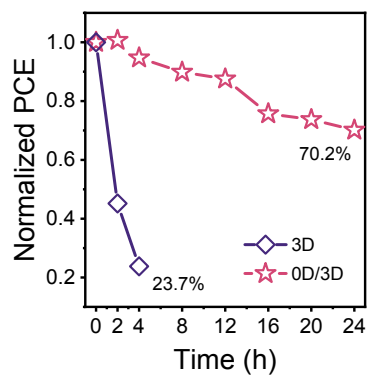


**Figure S13** Long-term stability of unencapsulated PSCs in ambient atmosphere with  $40\pm 5\%$  relative humidity under room temperature.